

Frequency-resolved Transient Absorption Spectroscopy for High Pressure System

Zi-Qian Cheng,¹ Xiao-Shuang Yin,² Liu-Xiang Yang,² and Hui Dong¹

¹*Graduate School of China Academy of Engineering Physics, Beijing 100193, China*

²*Center for High Pressure Science and Technology Advanced Research, Beijing 100193, China*

(*Electronic mail: hdong@gscaep.ac.cn)

(*Electronic mail: liuxiang.yang@hpstar.ac.cn)

Dynamics of materials under high-pressure conditions has been an important focus of materials science, especially in the timescale of pico- and femto-second of electronic and vibrational motion, which is typically probed by ultrafast laser pulses. To probe such dynamics, it requires an integration of high-pressure devices with the ultrafast laser system. In this work, we construct a frequency-resolved high-pressure transient absorption spectroscopy system based on a diamond anvil cell (DAC) with transmissive detection. In this setup, we use the narrowband laser as the pump beam and the supercontinuum white light as the probe beam. To effectively eliminate the scattering noise from the pump light, we design a double-chopper operating mode, which allows us to obtain signals in the complete frequency domain including the overlap region with the pump pulse. And we test system with Rhodamine B solution with the probe wavelength range of 450-750 nm and the 550nm pump, and observe that the intensity of the signal peak corresponding to the monomer at 560 nm continuously decreased relative to the signal peak corresponding to the dimer at 530 nm. This indicates that the portion of Rhodamine B molecules in the dimer form increases under increasing pressure. Additionally, we find two dynamic components of the signal peaks for both monomer and dimer, and the short-lifetime component increases as the pressure is increased, and the long-lifetime component decreases.

I. INTRODUCTION

With the advent of femtosecond pulse laser technology, transient absorption (TA) spectroscopy has developed rapidly and has been widely used in molecular biology, chemistry, and condensed matter physics. Its femtosecond time resolution enables to explore the charge and energy transfer dynamics in researches of photosynthetic proteins¹⁻⁴, organic molecules⁵, dyes⁶⁻⁸, semiconductor devices⁹⁻¹¹, and perovskites¹²⁻¹⁴. Currently, most of the applications remain confined to normal pressure environments. To extend spectroscopic methods into the high-pressure researches, it requires an integration of high-pressure apparatus with the spectroscopic detections. One of the possible apparatus is the diamond anvil cell (DAC)^{15,16}, which has played a crucial role in the field of high-pressure physics as a safe, low-cost, easily operable experimental device capable of applying pressures over 100 GPa¹⁷. It combines high pressure with high temperature, strong magnetic fields, and optical excitation, assisting researchers in exploring the physical properties of materials under various conditions¹⁶. The transparent windows on the both sides of DAC offer a possibility to integrate the laser pulse probe. However, due to the effects of light absorption and scattering by the diamonds within the DAC, the application of femtosecond pulsed for measurements of samples inside the DAC still faces many limitations.

There are already several successful experimental attempts to combine high pressure with spectroscopy¹⁸, including the detection of the absorption and photoluminescence spectra under pressure gradients¹⁹ with the spectrum filter²⁰. Due to the limitations of aperture and sample size in DAC, co-linearly arranging of the pump and probe beams of different wavelengths is typically used along with bandpass filters to

block scattered noise. In such a setup, it is hard to have the frequency resolution²¹.

To obtain dynamic information, it typically requires the spectrum overlap between the pump and probe pulse under resonant pump-probe conditions, where the scattering from the pump pulse results in significant amount of noise. To overcome such problem, we design a TA system with non-collinear geometry so that only a small portion of the pump light is scattered on the diamond into the probe light. By adding choppers in the both pump and probe beams, we further remove the scattering noise from the pump and obtain the spectrum of the pump scattering noise in real time and subtract it, such that a complete spectrum is obtained even when the spectrum of the pump beam is overlapped with the probe beam. With this setup, we use Rhodamine B in water as the test sample and observe clear spectral changes in the pressure range of 0.11-0.98 GPa. We find two ground-state-bleaching peaks corresponding to the Rhodamine B monomers and dimers, and their intensity changes with the increasing pressure. Such change characterize the process in which the Rhodamine B molecules in water gradually transform from monomers to dimers.

II. EXPERIMENTAL SET-UP

In Fig.1, we present the current setup of the frequency-resolved high-pressure transient absorption spectroscopy system. The light source for TA spectra is an 800-nm Ti:sapphire amplified pulsed laser which delivers pulses with the width of 35fs at a 10-kHz repetition rate. The output light is split into two parts: one beam (red lines) is used to generate a 550 nm pump pulse through an optical parametric amplifier, and the other beam (blue lines) is used to generate supercontin-

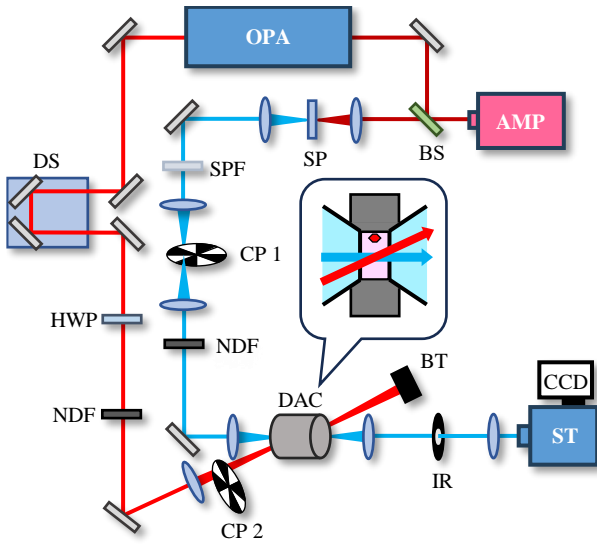


FIG. 1. The experimental setup of frequency-resolved high-pressure transient absorption spectroscopy. AMP: Ti:Sapphire amplifier laser system; OPA: optical parametric amplifier; BS: beam splitter; SP: sapphire window; SPF: short-pass filter; DS: delay stage; CP: chopper; HWP: half-wave plate; NDF: neutral density filter; DAC: diamond anvil cell; BT: beam trap; IR: iris; ST: spectrometer; CCD: charge coupled device camera. Magnified view: the sample cell structure, where the light blue area, dark gray area, pink area, and red hexagon represent the diamond, rhenium plate, Rhodamine B solution, and ruby, respectively. In the entire diagram, the dark red line, blue line, and red line represent the 800 nm fundamental pulse, the probe pulse, and the pump pulse, respectively.

uum white light via a 3 mm thick sapphire window as the probe pulse^{22,23}. The pump pulse is sent through an electronically controlled mechanical delay line to adjust the optical path length, thereby controlling the time delay between the pump and probe pulses reaching the sample. The probe light is incident vertically on the sample in the DAC with pulse energies of 0.58nJ, while the pump light is incident on the sample at an angle of approximately 15° to the normal with pulse energies of 9nJ. The polarization angle between the two beams is set to the magic angle to avoid noise caused by anisotropy of dipoles²⁴. We use lenses with focal lengths of 150 mm and 200 mm to focus the probe and pump pulses, respectively. This setup ensures that the two pulses can completely incident on the sample and the pump beam fully covers the probe beam at the sample location, maximizing the signal intensity. After passing through the sample, the probe pulse is led into the spectrometer and detected by a charge coupled device (CCD) camera.

The DAC with a culet diameter of 400 μm is used for the pressure loading. A Rhenium (Re) plate with thickness of 250 micrometers is used as the gasket. After pre-indentation to 70 μm , a 250 μm diameter hole is drilled into the gasket by laser to create a specimen chamber. The sample is placed inside the chamber, which is sandwiched by the diamonds. A ruby is placed in the chamber for the pressure calibration, and is positioned close to the edge of the chamber to avoid be-

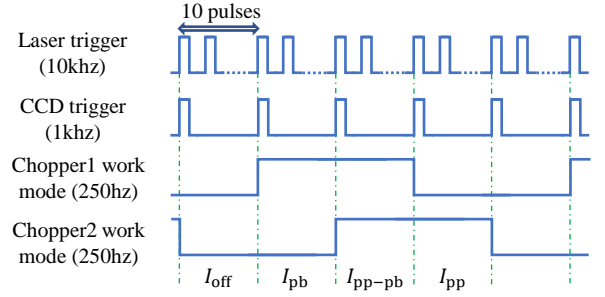


FIG. 2. Timing logic for double-chopper mode in our transient absorption system.

ing struck by any pump or probe pulses to generate artifacts in the signal. Between each set of TA spectra experiments, the DAC is removed from the optical path and pressurized. And the wavelength of the ruby fluorescence characteristic peak is measured to calibrate the pressure within the chamber for different experimental sets. To keep the sample in the liquid phase, we set the maximum pressure within the chamber as 1.0 GPa, with increments of 0.05 GPa for each experiments. In the liquid phase, the pressure distribution is uniform throughout the sample, and thus the position of the ruby does not affect the accuracy of the pressure measurement.

In the current setup, we utilize a double-chopper setup^{25,26} to eliminate the intense scattering noise generated when the pump pulse passes through the diamond in the DAC and other time-varying system noises. We balance the CCD's acquisition area size and sampling frequency, setting the exposure frequency to 1 kHz, which corresponds to capturing 10 pulses with each exposure. Two choppers, each with a frequency of 250 Hz, are positioned in the pump and probe beam paths, respectively. Due to the beam diameter of the supercontinuum white light being approximately 10 mm, we use a pair of achromatic lenses to focus and collimate the probe pulse before and after the chopper. This arrangement ensures that every 10 pulses are either completely blocked or fully transmitted by the chopper blades, with the chopper positioned at the focal points of the two lenses.

The laser trigger signal is processed into synchronization control signals for the CCD and choppers using a digital circuit board. By setting the relative phases, we set up the timing logic of our system as illustrated in Fig.2. The laser trigger signal with 10kHz is processed to generate the CCD signal at 1kHz to trigger the camera. The two choppers are triggered by the signal at 250Hz with different phase shift to form four different exposure combinations. Each acquisition cycle consists of these four exposures, pump-on and probe-on (I_{pp-pb}), pump-off and probe-on (I_{pb}), pump-on and probe-off (I_{pp}), and pump-off and probe-off (I_{off}). And the final TA signal is obtained as

$$\Delta T/T = \frac{(I_{pp-pb} - I_{pb}) - (I_{pp} - I_{off})}{I_{pb}}. \quad (1)$$

Scattering noise from the pump pulse is included in I_{pp-pb} and I_{pp} , and in turn eliminated from the final results.

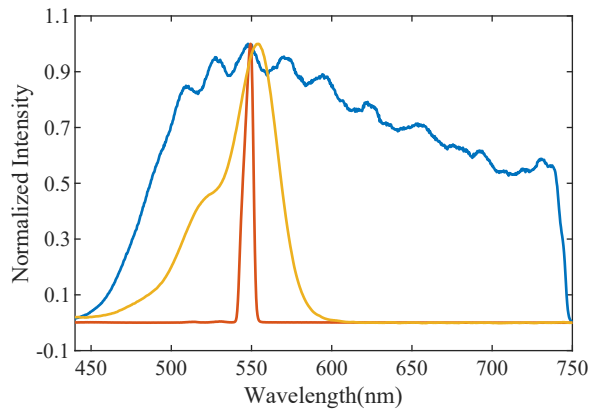


FIG. 3. The spectrum of the pump light (red line), the spectrum of the probe light (blue line), and the absorption spectrum of Rhodamine B under the ambient pressure (yellow line).

III. RESULTS AND DISCUSSIONS

With the current setup, we perform TA experiments on the sample with Rhodamine B in the water. A series of TA spectra are measured under different pressures ranging from 0.11 GPa to 0.98 GPa. The pump is a femtosecond laser pulse with central wavelength 550 nm and its spectral is shown as the red line in Fig.3. The supercontinuum white light with wavelength from 450 nm to 750 nm is used as the probe pulse, whose spectral is illustrated as the blue line in Fig.3. The absorption spectrum of Rhodamine B under the the ambient pressure is measured and shown in Fig.3 as the yellow line. The central wavelength of the pump pulse is chosen to ensure the effective excitation of the Rhodamine B molecules.

We show the obtained TA spectra for two typical pressures 0.11 GPa and 0.85 GPa in Fig.4(a) and (b) respectively with the current setup using double choppers. The data have been processed using the moving window smoothing technique along the wavelength axis to eliminate the oscillation interference caused by multiple reflections of the probe light on the diamond surface. The range of smoothing window is set to 5 adjacent pixels (2.5 nm for the wavelength range), ensuring effective noise filtering without losing signal peaks. Both TA spectra show the similar ground-state bleaching peaks at 560 nm. Comparing the signal dynamics in Fig.4(a) and (b) along the time delay axis, we observe that the relaxation is significantly faster at 0.85 GPa than that at 0.11 GPa. To show the effectiveness of our double chopper scheme, we also present the TA signals obtained using the traditional single-chopper method in Fig.4(c) and 4(d), where strong pump scattering noise is observed near 550 nm as the blue color data. In comparison, the scattering noise has been almost completely eliminated in Fig.4(a) and (b), with its intensity reduce to less than one-tenth of the maximum signal peak. The significant reduction of the noise related to the pump light scattering is one of advantages of the current setup, which allows the measurement of the full spectrum as presented in Fig.4(a) and (b). The results in Fig.4(a) are consistent with the previously reported TA spectra of Rhodamine B in water under ambient pressure⁸.

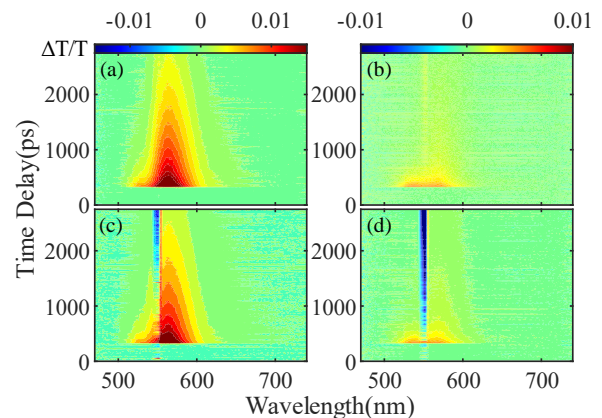


FIG. 4. The TA spectra of the Rhodamine B in water. (a) and (b) TA results at 0.11 GPa and 0.85 GPa under double-chopper mode, respectively. (c) and (d) TA results at 0.11 GPa and 0.85 GPa under the single-chopper mode, respectively.

In Fig.5, we show slice of the spectra at the time delay of 50 ps, and present the raw data in Fig.5 (a) and the normalized results in Fig.5 (b) for different pressures. The spectra show two distinct ground-state bleaching signal peaks at 560 nm (peak P1) and 531 nm (peak P2). Here the peak P1 at 560 nm corresponds to the main absorption peak of Rhodamine B monomers and the peak P2 at 530 nm corresponds to the absorption of dimers²⁷. The raw data shows that both intensities of the peak P1 and P2 decrease with the increase of pressure. The decay rate for the intensity of the peak P1 is larger than that of the peak P2, and in turn the intensity of the peak P2 is higher than that of peak P1 with the pressure higher than 0.74 GPa. The changes in the relative intensity of the signal peaks are attributed to the pressure-induced conversion of Rhodamine B molecules from monomers to dimers within the sample, which is consistent with previous experiments²⁸.

To track the impact of the pressure on the transient absorption, we select the localized signal within the range from 558 nm to 570 nm for Gaussian fitting to obtain the profile and center wavelength of peak P1. Then, we subtract the fitted Gaussian peak of P1 from the 520 - 548 nm signal and perform Gaussian fitting again to obtain the profile and center wavelength of P2. The change of the center wavelengths of P1 and P2 with pressure is shown in Fig.5(c) and (d). When the pressure exceeds 0.85 GPa, the intensity of P1 becomes so weak that it is completely overshadowed by P2. Therefore, the center wavelength of P1 is not shown at this pressure, and the center wavelength of P2 is directly obtained from the fitting of the original signal. As shown in Fig.5(c) and (d), with the pressure increase, the center of peak P1 redshifts from 562.0 nm to 565.4 nm, while the center of P2 redshifts from 523.7 nm to 540.2 nm. Such shift of the peak position may be caused by reduction of the reorganization energy of the transition due to the freezing of the freedom of the solution as the environment. With the pressure higher than 0.98 GPa, the solution is turned into the solid phase.

To extract the impact of the pressure on the dynamics, we plot the intensities of signals within a 5 nm wavelength range

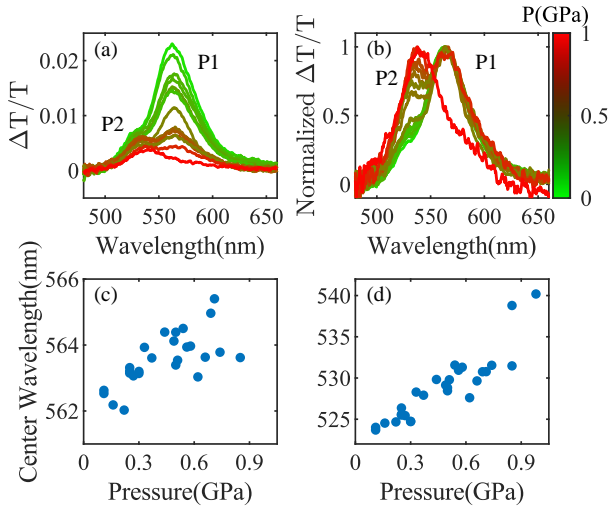


FIG. 5. The raw data (a) and normalized results (b) of TA spectra at the time delay of 50 ps under different pressure ranging from 0.11 GPa to 0.98 GPa. The pressure increases from the lowest (green line) to the highest (red line). And the changes of the central wavelengths of the peak P1 (c) and P2 (d) with increasing pressure.

around peak P1 and peak P2 as a function of the delay time, shown in Fig.6. These curves show a clear change of the dynamics of the signal with the increase of the pressure. The red curve (high pressure) exhibits a significantly deeper concavity compared to the green curve (low pressure). To quantitatively characterize these signals, we decompose the intensity changes of the peak P1 and P2 into two kinetic components and display the changes of their amplitude and lifetimes with pressure in Fig.7 by fitting the dynamics with the formula $\Delta T/T = A_{P_i\text{-slow}} \exp(-t/\tau_{P_i\text{-slow}}) + A_{P_i\text{-fast}} \exp(-t/\tau_{P_i\text{-fast}})$ ($i = 1, 2$). The trends of the fitting parameters for peak P1 and peak P2 are represented by the red and purple lines, respectively.

As shown in Fig.7(a), (b), (c), and (d), the amplitudes of the fast components of both peaks increase rapidly with increasing pressure, while the amplitudes of the slow components decrease. Such trend of shifting from the slow component to the fast component is consistent with the data within 1000 ps of the time delay in Fig.6.

In terms of lifetime, Fig.7(e) and (g) show almost no changes in the lifetime of the fast component of the single peaks with the changing pressure. Such an observation indicates that the kinetic mechanism of the rapid decay is not affected by the pressure. However, both the lifetime of the slow components in Fig.7(f) and (h) increase rapidly as the pressure rises. This lifetime is close to the fluorescence lifetime of Rhodamine B in water under ambient pressure²⁹.

We attribute the fast component to the inter-molecule interaction, whose amplitude is strongly affected by the pressure due to the change in molecular distance between the molecules. As the molecular distance decreases, more excited-state energy is transferred to solvent molecules through inter-molecular interactions instead of intra-molecular relaxation. However, the dynamics of this

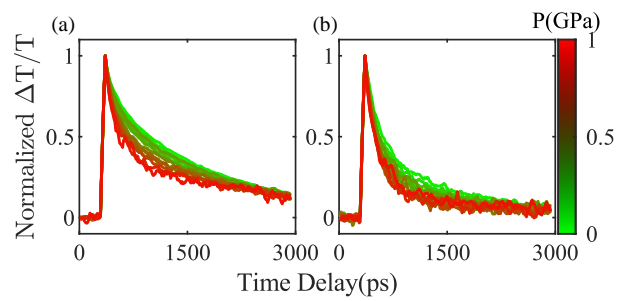


FIG. 6. The relaxation of the peak P1 (a) and peak P2 (b) with time delay. The data in the figure are normalized by the intensity at the time delay when the pump and probe pulses are completely overlapped. The pressure increases from the lowest (green line) to the highest (red line).

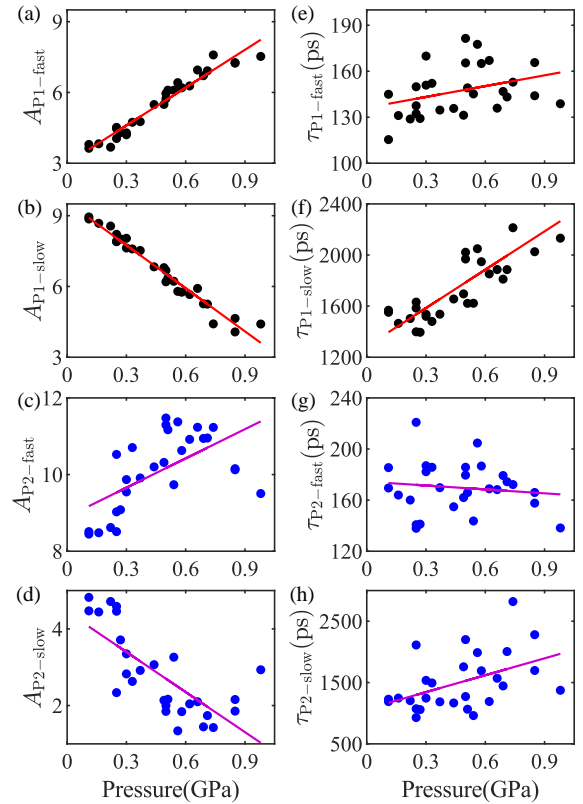


FIG. 7. The amplitudes and lifetimes of the peak P1 and peak P2 as a function of pressure. (a), (b), (e) and (f) Pressure-induced changes in amplitude and lifetime of the fast and slow component of the peak P1. The red lines show the trend of changes. (c), (d), (g) and (h) Pressure-induced changes in amplitude and lifetime of the fast and slow component of the peak P2. The purple lines represent the trend of changes

channel remain unchanged, as indicated by the consistency of its lifetime across different pressures.

For the slow component, we believe it represents intra-molecular relaxation, which is determined by the molecular structure of Rhodamine B. The pressure-induced transition of rhodamine molecules from monomers to dimers leads to an

increase of the intramolecular relaxation lifetime³⁰, which is consistent with the results shown in Fig.7(f) and (h). The amplitude of this relaxation process decreases as the contribution of inter-molecular interactions increases. At the same time, with the increase of the pressure, the solution transitions from the liquid phase to the solid phase, where some of the molecular degrees of the freedom is frozen and in turn result in longer lifetime. Indeed, we observe a substantial decrease in their absorption of the pump light when the pressure exceeds 0.98 GPa, due to the impending phase transition of the sample from the liquid to the solid phase.

IV. CONCLUSIONS

In conclusion, we construct a frequency-resolved high-pressure transient absorption spectroscopy system and conduct tests using Rhodamine B in water as the sample. This system uses the narrowband pulse as the pump beam and the supercontinuum white light as the probe beam, allowing for the acquisition of complete spectral signals in the 450-750 nm range, as well as performing dynamic analysis. By utilizing a double-chopper setup, the system effectively mitigates the impact of pump light scattering on the measurement results, allowing the measurement of the full TA spectrum when the pump and probe pulse have spectral overlap. This technique significantly extends the system's usability, making it possible to investigate the dynamic processes following resonant excitation under high-pressure conditions. The system is potentially applicable to samples that allow for stable light transmission, such as liquid samples and thin films.

ACKNOWLEDGMENTS

This work is supported by the Innovation Program for Quantum Science and Technology (Grant No. 2023ZD0300700), and the National Natural Science Foundation of China (Grant Nos. U2230203, U2330401, and 12088101).

AUTHOR DECLARATIONS

Conflict of Interest

The authors have no conflicts to disclose.

Author Contributions

Zi-Qian Cheng: Design and construction of the experimental system; Data acquisition (equal); Formal analysis (equal); Manuscript writing - review and editing (equal). **Xiao-Shuang Yin:** Data acquisition (equal); Manuscript review and editing (supporting). **Liu-Xiang Yang:** Conceptualization (equal); Formal analysis (equal); Manuscript review and

editing (supporting). **Hui Dong:** Conceptualization (equal); Formal analysis (equal); Funding acquisition (lead); Project administration (lead); Writing - review and editing (lead).

DATA AVAILABILITY

The data that support the findings of this study are available from the corresponding author upon reasonable request.

- ¹R. Berera, R. van Grondelle, and J. T. M. Kennis, *Photosynth. Res.* **101**, 105 (2009).
- ²R. Croce, M. G. Muller, R. Bassi, and A. R. Holzwarth, *Biophys. J.* **80**, 901 (2001).
- ³M. Kaucikas, D. Nurnberg, G. Dorlhiac, A. W. Rutherford, and J. J. van Thor, *Biophys. J.* **112**, 234 (2017).
- ⁴N. Zamzam, R. Rakowski, M. Kaucikas, G. Dorlhiac, S. Viola, D. J. Nurnberg, A. Fantuzzi, A. W. Rutherford, and J. J. van Thor, *Proc. Natl. Acad. Sci.* **117**, 23158 (2020).
- ⁵J. R. Hunt and J. M. Dawlaty, *J. Phys. Chem.* **123**, 10372 (2019).
- ⁶L. Jiang, W. Liu, Y. Song, X. He, Y. Wang, and Y. Yang, *Appl. Phys. B* **116**, 271 (2013).
- ⁷A. L. Dobryakov, S. A. Kovalenko, and N. P. Ernsting, *J. Chem. Phys.* **123**, 044502 (2005).
- ⁸P. Maly, J. Ravensbergen, J. T. M. Kennis, R. van Grondelle, R. Croce, T. Mancal, and B. van Oort, *Sci. Rep.* **7**, 43484 (2017).
- ⁹H. Ohkita and S. Ito, *Polymer* **52**, 4397 (2011).
- ¹⁰J. Ravensbergen, F. F. Abdi, J. H. van Santen, R. N. Frese, B. Dam, R. van de Krol, and J. T. M. Kennis, *J. Phys. Chem. C* **118**, 27793 (2014).
- ¹¹K. E. Knowles, M. D. Koch, and J. L. Shelton, *J. Mater. Chem. C* **6**, 11853 (2018).
- ¹²N. Yarita, H. Tahara, T. Ihara, T. Kawawaki, R. Sato, M. Saruyama, T. Teranishi, and Y. Kanemitsu, *J. Phys. Chem. Lett.* **8**, 1413 (2017).
- ¹³L. Wang, C. McCleese, A. Kovalsky, Y. Zhao, and C. Burda, *J. Am. Chem. Soc.* **136**, 12205 (2014).
- ¹⁴E. Serpetzoglou, I. Konidakis, G. Kakavelakis, T. Maksudov, E. Kymakis, and E. Stratakis, *ACS Appl. Mater. Inter.* **9**, 43910 (2017).
- ¹⁵P. W. Bridgman, *P. Roy. Soc. A-math. Phys.* **203**, 1 (1950).
- ¹⁶W. A. Bassett, *High Pressure Res.* **29**, 163 (2009).
- ¹⁷A. Jayaraman, *Rev. Mod. Phys.* **55**, 65 (1983).
- ¹⁸Q. Zhou, B. Cao, Y. Li, B. Li, H. Yin, J. Gao, M. Jin, Y. Shi, C. Liu, and D. Ding, *Appl. Phys. Lett.* **117**, 063101 (2020).
- ¹⁹D. Liu, D. Dong, Z. Zhang, Y. He, Z. Li, J. Niu, N. Yu, and H. Jia, *Opt. Mater.* **146**, 114537 (2023).
- ²⁰Y. L. Wu, X. Yin, J. Z. L. Hasaen, Z. Y. Tian, Y. Ding, and J. Zhao, *Rev. Sci. Instrum.* **92**, 113002 (2021).
- ²¹Q. Li, L. Sui, G. Niu, J. Jiang, Y. Zhang, G. Wu, M. Jin, and K. Yuan, *J. Phys. Chem. C* **124**, 11183 (2020).
- ²²A. Dubietis and A. Couairon, *Ultrafast Supercontinuum Generation in Transparent Solid-State Media*, SpringerBriefs in Physics (Springer International Publishing, 2019).
- ²³A. Dharmadhikari, F. Rajgara, and D. Mathur, *Appl. Phys. B* **80**, 61 (2005).
- ²⁴S. Schott, A. Steinbacher, J. Buback, P. Nuernberger, and T. Brixner, *J. Phys. B* **47**, 124014 (2014).
- ²⁵B. Tobias, M. Tomáš, I. V. Stiopkinand, and G. R. Fleming, *J. Chem. Phys.* **121**, 4221 (2004).
- ²⁶J. Yue, L. Zhou, P. Su, and W. Zhang, *Chem. Phys. Lett.* **802**, 139766 (2022).
- ²⁷T. Fujii, H. Nishikiori, and T. Tamura, *Chem. Phys. Lett.* **233**, 424 (1995).
- ²⁸E. R. Roberts and H. G. Drickamer, *J. Phys. Chem.* **89**, 3092 (1985).
- ²⁹A. S. Kristoffersen, S. R. Erga, B. Hamre, and Ø. Frette, *J. Fluoresc.* **24**, 1015 (2014).
- ³⁰F. del Monte and D. Levy, *J. Phys. Chem. B* **102**, 8036 (1998).